The Astrophysical Journal, 573:191–198, 2002 July 1

GALACTIC STARBURST NGC 3603 FROM X-RAYS TO RADIO

A. F. J. Moffat,[1] M. F. Corcoran,[2,3] I. R. Stevens,[4] G. Skalkowski,[1] S. V. Marchenko,[1,5] A. Mücke,[1,6] A. Ptak,[7] B. S. Koribalski,[8] L. Brenneman,[3] R. Mushotzky,[3] J. M. Pittard,[9] A. M. T. Pollock,[10] and W. Brandner[11]

Received 2001 April 6; accepted 2002 March 5

ABSTRACT

NGC 3603 is the most massive and luminous visible starburst region in the Galaxy. We present the first *Chandra* ACIS-I X-ray image and spectra of this dense, exotic object, accompanied by a deep centimeter-wavelength Australia Telescope Compact Array radio image at similar $\lesssim 1''$ spatial resolution and *Hubble Space Telescope*/ground-based optical data. At the S/N > 3 level, *Chandra* detects several hundred X-ray point sources (compared to the three distinct sources seen by *ROSAT*). At least 40 of these sources are definitely associated with optically identified cluster O- and W-R–type members, but most are not. A diffuse X-ray component is also seen out to $\sim 2'$ (4 pc) from the center, probably arising mainly from the large number of merging/colliding hot stellar winds and/or numerous faint cluster sources. The point-source X-ray fluxes generally increase with increasing bolometric brightnesses of the member O/W-R stars, but with very large scatter. Some exceptionally bright stellar X-ray sources may be colliding wind binaries. The radio image shows (1) two resolved sources, one definitely nonthermal, in the cluster core near where the X-ray/optically brightest stars with the strongest stellar winds are located, (2) emission from all three known proplyd-like objects (with thermal and nonthermal components), and (3) many thermal sources in the peripheral regions of triggered star formation. Overall, NGC 3603 appears to be a somewhat younger and hotter scaled-down version of typical starbursts found in other galaxies.

Subject headings: open clusters and associations: individual (NGC 3603) — stars: early-type — stars: winds, outflows

1. INTRODUCTION

Hot stars, by means of the massive supersonic winds and the supernovae they produce, have a profound influence on their environment and on galactic and chemical evolution in the universe. A sufficient density of massive stars can drive galactic-scale outflows, such as that seen in M82. While many advances have been made in the study of such starburst galaxies, they are typically too distant to study in great detail. Consequently, any local analogs, such as giant H II regions in our own Galaxy and in the Magellanic Clouds, are of great interest.

Giant H II regions—particularly if relatively compact yet nearby—provide nearly coeval samples of large numbers of resolved massive stars. Deep X-ray imaging is an efficient way to measure the X-ray properties of a viable, homogeneous sample of OB/W-R stars. We have therefore used the *Chandra* X-ray satellite to image NGC 3603—the brightest, most luminous visible giant H II region with near-solar abundance in the Galaxy, at an adopted distance of 7 kpc (Moffat 1983; Moffat, Drissen, & Shara 1994; Drissen et al. 1995; Brandl et al. 1999). The *Chandra* observations are complemented by centimeter-wavelength radio imaging at the Australian Telescope Compact Array (ATCA) and by optical observations using the *Hubble Space Telescope* (*HST*) and ground-based telescopes. Such multiwavelength data, all at similar spatial resolution, provide a clear advantage when it comes to understanding the physics of starburst regions. For example, X-ray and radio emission mechanisms are often related (e.g., in regions of shocked gas), and optical data are indispensable for identifying X-ray sources. This preliminary study will show how X-ray and radio properties of the cluster relate to the physical properties of the stars and gas in a starburst region.

2. OBSERVATIONS

We have obtained a deep, 50 ks, uninterrupted pointing at NGC 3603 with ACIS-I on *Chandra* in 2000 May (cycle AO1), with a spatial resolution of $\sim 1''$. The ACIS-I image was created from the standard photon events after they were cleaned to remove photons falling near node boundaries or near other bad pixel regions. Inspection of X-ray light curves of a region centered on NGC 3603 and on a background region to the north of the cluster indicates that there is no evidence for the presence of flares, so that no time

[1] Département de Physique, Université de Montréal, C.P. 6128, Succ. Center-Ville, Montréal, QC H3C 3J7, Canada; and Observatoire du mont Mégantic; moffat@astro.umontreal.ca, sergey@astro.umontreal.ca, gwen@astro.umontreal.ca.

[2] Universities Space Research Association, 7501 Forbes Boulevard, Suite 206, Seabrook, MD 20706.

[3] Laboratory for High Energy Astrophysics, Goddard Space Flight Center, Greenbelt, MD 20771; corcoran@barnegat.gsfc.nasa.gov, bren@lhea1.gsfc.nasa.gov, richard@xray-5.gsfc.nasa.gov.

[4] School of Physics and Astronomy, University of Birmingham, Birmingham B15 2TT, UK; irs@star.sr.bham.ac.uk.

[5] Now at Department of Physics and Astronomy, Western Kentucky University, Thompson Complex Central Wing, Bowling Green, KY 42101-3576; sergey@astro.wku.edu.

[6] Now at Institut für Theoretische Physik, Ruhr-Universität Bochum, D-44780, Germany; afm@tp4.ruhr-uni-bochum.de.

[7] Physics Department, Carnegie Mellon University, 5000 Forbes Avenue, Pittsburgh, PA 15213; ptak@cmu.edu.

[8] Australia Telescope National Facility, CSIRO, P.O. Box 76, Epping 1710, Australia; baerbel.koribalski@atnf.csiro.au.

[9] Department of Physics and Astronomy, University of Leeds, Leeds LS2 9JT, UK; jmp@ast.leeds.ac.uk.

[10] Computer and Scientific Co. Ltd., 230 Graham Road, Sheffield S10 3GS, UK; andy@westwood.demon.co.uk.

[11] Institute for Astronomy, University of Hawaii, 2680 Woodlawn Drive, Honolulu, HI 96822; brandner@ifa.hawaii.edu.

intervals need to be excluded. The cleaned events were then spatially binned to produce an image of the central $3'.6 \times 3'.6$ at the full resolution of ACIS ($0''.492$ pixel^{-1}). We corrected the image for exposure variations across the detector and smoothed the resulting image with an adaptive filter. The smoothed, cleaned image is shown in Figure 1 (*left*).

In addition to the X-ray data, we present radio data from four 12 hr shifts with the ATCA at 3 and 6 cm wavelengths taken in 2000 February, April, June, and September (see Mücke et al. 2002a), resulting in a resolution of $1''.0 \times 0''.8$ at 3 cm with a noise level of $\sim$0.15 mJy. The radio data use only the longest baselines (greater than 25 kλ); this will tend to emphasize the small-scale structure. Finally, we complement the X-ray and radio data by a broadband visual *HST*/Wide Field Planetary Camera (WFPC) image of the central core at $0''.1$ resolution, along with a $1''$ resolution image of the whole cluster and its surroundings (i.e., similar to the resolution of the X-ray and radio data) from the 0.9 m telescope at the Cerro Tololo Inter-American Observatory (CTIO).

Figure 1 shows overview linear intensity scale images centered on NGC 3603, in (1) X-rays (0.5–10 keV, i.e., 24–1.2 Å) and (2) ground-based medium-band optical light ($\lambda_c = 0.465$ μm $= 4650$ Å), both at the same size, scale, and resolution ($\sim 1''$). Also shown superposed (*blue contours*) are the $\lambda = 3$ cm $= 3 \times 10^8$ Å radio data, which have been slightly adjusted in right ascension (R.A.) and declination (decl.) so that the radio flux of the proplyd-like objects P1 and P2 (P3 is outside the *HST* field in Hα) coincide best with their *HST* positions in Hα emission (see Mücke et al. 2002a). Figure 2 is an enlargement of the central field of Figure 1, with superposed deconvolved ACIS-I X-ray (*green*) and smoothed *HST* optical (*red*) images and 3 cm radio contours. The *Chandra* image was shifted in R.A. and decl. by less than $0''.5$ to bring the brightest, most obvious *HST* sources in good positional agreement. Stellar coincidences between X-ray and optical appear in bright yellow.

3. RESULTS AND DISCUSSION

3.1. *O Star X-Ray Spectral Properties*

In principle, it is possible to obtain X-ray spectra for bright detected sources directly from the ACIS data, since the CCD detectors measure the pulse-height amplitude for each detected photon from each source. In practice, this is difficult to do directly, since the brightest sources in the image suffer from pileup (in which two or more photons arrive at a single pixel in one readout cycle and are counted as a single photon event), which causes a loss of flux and an increase in high-energy photons at the expense of low-energy photons. Individual fainter sources that do not suffer from pileup do not have enough counts for us to derive a well-defined X-ray spectrum. Assuming that stars of similar spectral type should possess similar X-ray spectra, we have defined a composite stellar X-ray spectrum by extracting spectra for individual faint sources of similar spectral types and coadding the spectra to produce an unpiled spectrum of sufficient significance. There are seven member stars of early O spectral type in the core of NGC 3603 that are fairly well resolved in the ACIS image and detected at a signal-to-noise ratio level greater than 3, yet do not suffer from serious pileup. These are H19, H49, H50, H52, H58, H61, and H62 from Moffat et al. (1994); see Figure 1.

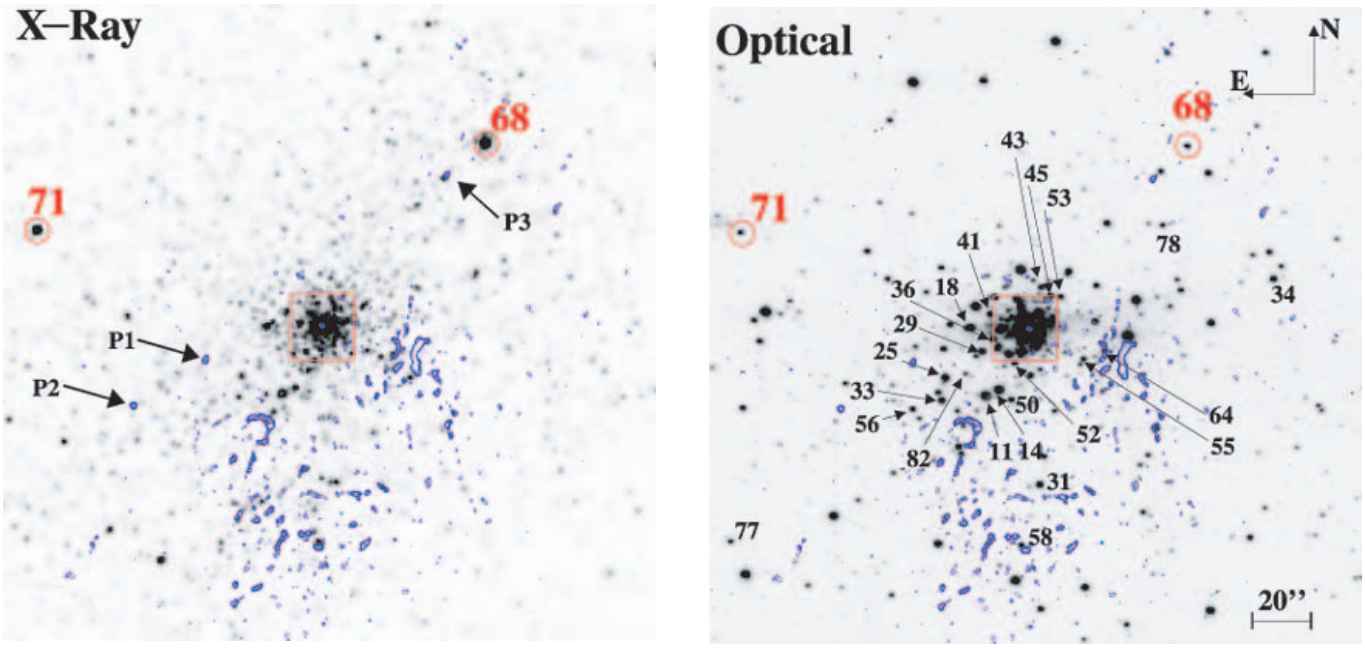

FIG. 1.—Overview $3'.6 \times 3'.6$ (7.3 × 7.3 pc at the adopted distance for NGC 3603 of 7.0 kpc) maps in linear intensity centered on NGC 3603 in smoothed X-ray flux (corrected for exposure variations and cleaned of detector artifacts) (*left*) and ground-based optical emission (*right*). Both have the same scale and resolution ($\sim 1''$). Radio contours (*blue*, resolution also $\sim 1''$, with contour levels of 3, 5, 7, and 10 σ, where 1 $\sigma = 1.5 \times 10^{-4}$ Jy beam^{-1}) are superposed on the left and right panels, respectively, with the three proplyd-like objects indicated. Identifications (cf. Melnick et al. 1989) of member OB stars outside the central core and with detected *Chandra* X-ray fluxes are indicated in the right panel (two stars are repeated in the left panel for orientation purposes). The central red boxes indicate the enlarged region in Fig. 2.

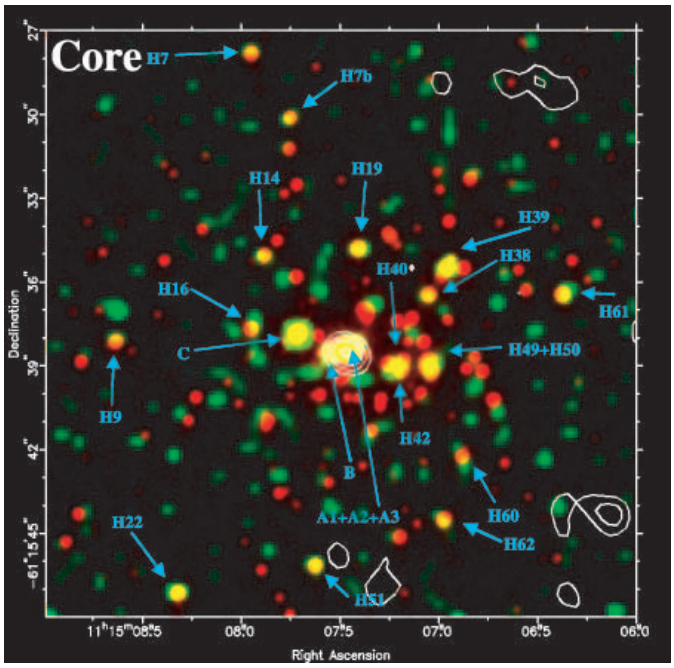

FIG. 2.—Enlarged 21″ × 21″ (0.71 × 0.71 pc) region centered on NGC 3603, with superposed *Chandra* X-ray (*green*) and *HST* optical (*red*) images. The *HST* image has been Gaussian smoothed to a resolution of ~0.″5, to match the deconvolved and Gaussian-smoothed X-ray image. Radio contours in steps as in Fig. 1 are superposed. Overlapping (within a PSF radius) X-ray and optical sources become bright yellow; these are identified with prefix H, as members of NGC 3603 (Moffat et al. 1994), with star H7b added. Note that the bright central stars A1, A2, A3, B, and C are H30, H31, H26, H23, and H18 of Moffat et al. (1994). When more than one star coincides within a PSF radius, appropriate identification is given. Epoch 2000 equatorial coordinates are indicated.

Before extracting and coadding the spectra for these seven sources, we attempted to correct the detected X-ray photons for the effects of charge transfer inefficiency (CTI), in which the pulse-height distribution changes as the charge migrates from the source position to the CCD readout. This is of concern here, since the distortions due to CTI will be different for each of our sources, depending on how far each source is from the chip readout. To minimize the effects of CTI on the extracted stellar X-ray spectrum, we corrected the individual photon events using the algorithm of Townsley et al. (2000).

We extracted the X-ray spectra from the cleaned, CTI-corrected photons for these seven stars using extraction regions of about 1″ in radius. The composite spectrum is shown in Figure 3. We extracted background from the cleaned, CTI-corrected photon event file in a nearby source-free circular region of radius 17″. We binned the composite early O star spectrum so that each bin had a minimum of 10 counts, and we then fit the binned, background-subtracted spectrum using a single-temperature Mewe, Kaastra, & Liedahl (1995) emission model plus absorption by overlying cool material. The best fit for this model is shown superposed in Figure 3. The derived temperature is $kT = 0.85 \pm 0.1$ keV and $N_{\rm H} = 1.3 \pm 0.1 \times 10^{22}$ cm^{-2} at the 90% confidence level. The fit using this single-component model is formally unacceptable (reduced $\chi^2 = 1.29$); most of the contribution to χ^2 is produced by an apparent excess at $E > 3$ keV, which is not matched by the single-component emission model.[12] The flux for this model is $\sim 6 \times 10^{-14}$ ergs cm^{-2} s^{-1} in the energy range 0.5–10 keV, suggesting that each star has an average X-ray luminosity of $\sim 5 \times 10^{31}$ ergs s^{-1} for an assumed distance of 7 kpc.

[12] A multitemperature model (e.g., as for three of the Orion Trapezium stars; Schulz et al. 2001) would undoubtedly fit better; however, we consider this to be overanalysis in the context of this overview paper.

3.2. *Stellar Point-Source Members of NGC 3603*

The standard ACIS processing provides a source list produced by running a local cell-detection algorithm (the CELLDETECT tool from the *Chandra* Interactive Analysis of Observations [CIAO] version 1.1) with the local signal-to-noise ratio set to 3. This is probably adequate near the center of the field but may be less acceptable farther off-axis, since sensitivity varies with off-axis position. The standard source list contains 174 sources. A casual inspection of the source positions compared to the adaptively smoothed exposure-corrected image suggests that the simple cell-detection algorithm probably misses about 30%–50% of the sources visible to the eye. We also analyzed the field using the wavelet source detection tool, WAVDETECT, available in CIAO version 2.2. The wavelet-detection algorithm finds about 50 more sources compared to the local cell-detection algorithm, although the X-ray fluxes from this are less reliable than with CELLDETECT. As an alternative, we wrote our own simple cell-detection algorithm, which is similar, but not identical, to the CIAO CELLDETECT algorithm. First, our algorithm calculates the background level across the image iteratively, omitting potential point sources. Then, it assesses the significance of approximately pointlike events using a specified statistical threshold (3 σ in our case), calculated after Gehrels (1986). Each pointlike event is recognized as such after integrating the counts within a given distance ($r = 2, 3, 4, \ldots$ pixels) from the potential source. Finally, the algorithm compiles a list of spatially independent events (simply those that are separated by $d \geq r$). Using $r = 4$ pixels, we found 384 sources in the whole field. A more detailed analysis of the X-ray properties of detected X-ray

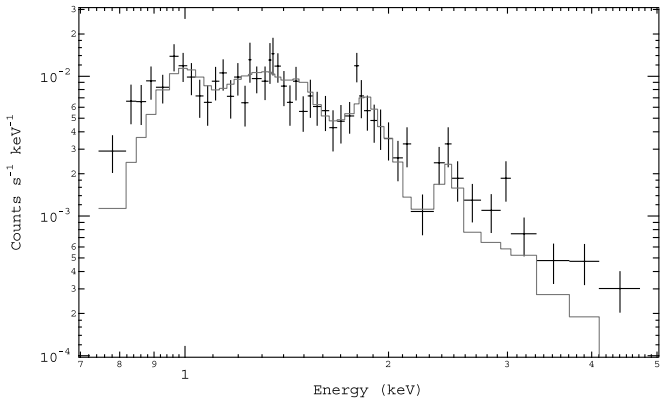

FIG. 3.—Composite summed X-ray spectrum of seven fairly well resolved early O stars that do not suffer pileup in the core of NGC 3603, with model superposed. See text for details.

sources, their identifications, and inclusion of upper limits for optical stars not detected in our *Chandra* pointing is currently underway; for the remainder of this paper, we consider for analysis the source list derived from our own simple cell-detection algorithm, which yields the most sources.

In Figure 4 we show a plot of X-ray (unabsorbed) versus bolometric luminosity of detected point sources labeled in Figures 1 and 2. This sample contains all the sources for which X-ray fluxes are detected above the $\sim 3\ \sigma$ level *and* for which optical magnitudes/colors/spectral types reveal their membership as OB/W-R stars in NGC 3603; cf. Melnick, Tapia, & Terlevich (1989) and G. Skalkowski et al. 2002 (in preparation) for stars outside the dense core and Moffat et al. (1994) and Drissen et al. (1995) for the cluster center. Cluster membership is well established in the area of Figure 1 (except possibly for some fainter stars in the core) down to $V \sim 15$ mag. This corresponds to $L_{\rm bol} \sim 8 \times 10^{38}$ ergs s^{-1}, so that Figure 4 is limited almost entirely by $L_{\rm X}$. To derive $L_{\rm bol}$ for the member stars, we adopted the visual absolute magnitudes M_V from the aforementioned photometric studies. Then, with constant bolometric correction (BC $= M_V - M_{\rm bol} = 4.5$ mag)[13] and distance 7 kpc, we derived the $M_{\rm bol}$ and $L_{\rm bol}$. For conversion of ACIS count rate to flux $L_{\rm X}$, we assumed a Raymond-Smith thermal spectrum with a temperature of 0.7 keV, typical of the X-ray temperatures of single massive stars (see, e.g., Corcoran et al. 1994) and consistent with other analyses (Chlebowski, Harnden, & Sciortino 1989; Berghöfer et al. 1997; this paper, see § 3.1), and $N_{\rm H}$ derived using the relation $N_{\rm H} = 5.8 \times 10^{21} E(B-V)$ (Bohlin, Savage, & Drake 1978). Use of a Mewe et al. (1995) model instead of a Raymond-Smith model would lead to negligible changes here. Note that an increase to $kT = 1.0$ keV would increase the absorbed X-ray fluxes in the 0.5–10 keV band by ~15%, which is relatively unimportant here. The unabsorbed ("dereddened") X-ray fluxes are much more sensitive to the assumed spectral shape. However, further refinement is not justified with the present non–piled-up spectra, which have only ~100 counts each at best. We consider an apparent association between point X-ray and optical sources only if the separation does not exceed one resolution element, thus probably missing several potential associations (especially in Fig. 2). Neglecting this, we plot in Figure 4 ~45 point-source members of NGC 3603 with almost certain X-ray/optical associations. Of particular note are the following:

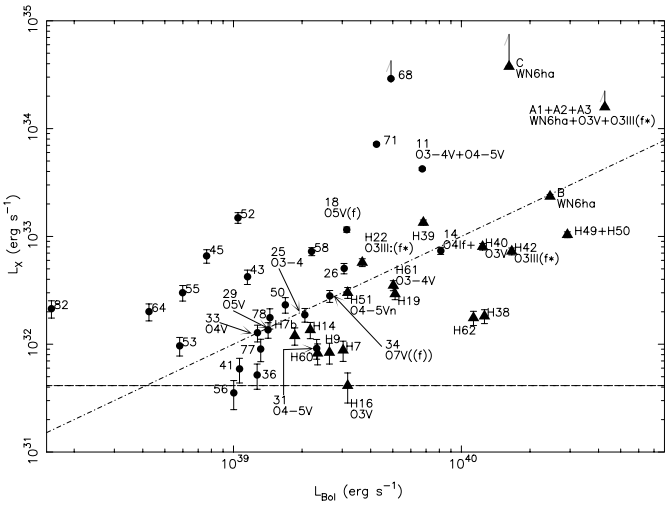

FIG. 4.—X-ray vs. bolometric luminosity of all X-ray–detected member hot stars of NGC 3603 (labeled stars in right panel of Fig. 1 [*circles*] and in Fig. 2 [*triangles*]). MK spectral types are indicated when available, from Drissen et al. (1995) and G. Skalkowski et al. 2002 (in preparation). The dash-dotted line follows the relation $L_{\rm X}/L_{\rm bol} = 10^{-7}$. The horizontal dashed line shows the 3 σ detection limit for stars on the ACIS-I image. We make no attempt to plot individual stars below this limit. Since no correction for pileup has been applied, the derived X-ray luminosities for stars brighter than $L_{\rm X} \sim 10^{34}$ ergs s^{-1} are underestimated, roughly as indicated by the arrows. Error bars are not visible when they are smaller than the size of the symbol.

1. X-ray flux generally increases directly with bolometric flux in the usual way (e.g., Seward & Chlebowski 1982; Chlebowski et al. 1989; Berghöfer et al. 1997), i.e., $L_{\rm X} \sim 10^{-7} L_{\rm bol}$, extended here to higher bolometric luminosities. However, there are at least 2 orders of magnitude scatter in the X-ray flux around this simple scaling relation. The large scatter appears to be intrinsic to the NGC 3603 stars, since we only consider members of NGC 3603, with field stars excluded.

2. All of the brightest early O stars and all three of the W-R stars are seen in X-rays. These relatively H-rich W-R stars are by far the brightest optical sources in the cluster, all located in the core. They are probably main-sequence stars of extremely high luminosity with strong wind-produced emission lines, similar to the three bright H-rich W-R stars in the R136 core of 30 Dor (De Koter, Heap, & Hubeny 1997; Crowther & Dessart 1998). Thus, the three W-R stars in NGC 3603 probably do not behave like genuine highly evolved (Galactic, single) W-R stars of the WN sequence, for which $L_{\rm X}$ and $L_{\rm bol}$, ranging over 10^{31}–10^{34} and 10^{38}–$10^{39.5}$ ergs s^{-1}, respectively, are uncorrelated (Wessolowski 1996).

3. The two optically bright late O/early B supergiants H1(OC9.7 Ia) and H5(= Sher 25, B1.5 Ia, with the SN 1987A–like ring structures; see Brandner et al. 1997), located ~20″ outside the cluster core, have no significant X-ray detection. This is likely a consequence of their relatively low $L_{\rm bol}$ combined with their slower winds. These two stars

[13] This is reasonable, since most of the detected stars are of early O type or H-rich WNL and hence, nearly constant bolometric correction (BC).

probably belong to a more extended, slightly older population, compared to the extreme youth of the rest of the known bright members of NGC 3603.

4. Several sources have relatively outstanding X-ray fluxes[14] for their L_{bol}; in approximate order of decreasing L_X/L_{bol}: (1) the W-R star C, which might be the suspected long-period (hundreds of days) W-R binary of Moffat & Niemela (1984), possibly similar to the extremely X-ray bright H-rich WNL star W-R 25 in the Carina Nebula (Seward & Chlebowski 1982); (2) MTT 68 and MTT 71 (Melnick et al. 1989; see Fig. 1), two heavily reddened ($E_{B-V} \sim 1.93$, compared to the cluster core with $E_{B-V} = 1.44$) member OB stars located over 1′ (2 pc projected separation) from the cluster core; these two stars also stand out on *ROSAT* X-ray Position Sensitive Proportional Counter (PSPC) images; (3) the W-R star A1 (although confused in X-rays with the two nearby but optically resolved O3 stars A2 and A3), which is now known to be a 3.771 day binary (Moffat & Niemela 1984; A. F. J. Moffat et al. 2002, in preparation); and (4) the O3-4V + O4-5V double-line system, star number 11 in Figure 1 (*right*). Whether all or most of the enhanced X-ray emission arises from colliding winds in close binaries remains to be demonstrated.

5. Some remaining X-ray point sources have no obvious bright optical counterparts, yet their frequency increases toward the cluster center. Some of these might be correlated with optically faint but active pre–main-sequence stars (e.g., Brandl et al. 1999).

6. Two significant but faint discrete radio sources above the noise level lie in the central cluster region of Figure 2. Of particular note is the stronger source, practically in the cluster center at the position of stars A1+A2+A3+B. Its contour lines at $\lambda 3$ and 6 cm appear slightly elongated [major and minor axes of $(1\farcs32 \pm 0\farcs01) \times (1\farcs09 \pm 0\farcs01)$, compared to a beam size of $(0\farcs94 \times 0\farcs77)$ at 3 cm and $(1\farcs86 \pm 0\farcs04) \times (1\farcs28 \pm 0\farcs02)$, cf. $(1\farcs53 \times 1\farcs23)$ at 6 cm]. Its spatially integrated flux is $S_\nu = 3.3 \pm 0.3$ mJy at 3 cm, as expected if arising in the winds of ~10–20 hot O/WNL stars as a result of thermal bremsstrahlung (using the model of Wright & Barlow 1975 together with the Kudritzki, Pauldrach, & Puls 1987 law, typical wind velocities of 1000 km s^{-1}, and stellar radii of 10 $R_\odot$). The power-law index between 3 and 6 cm is $\alpha = -0.2 \pm 0.2$ (for $S_\nu \propto \nu^\alpha$), significantly smaller than $\alpha = 0.6$ expected for the thermal emission from hot stellar winds. This, along with its extended nature, suggests the presence of a nonthermal radio component, possibly arising in zones of colliding winds (although without an obvious X-ray counterpart). The second central radio source is located ~3″ west of the first source and is only seen at 6 cm, but with nearly the same flux as the first source, near stars H49+H50. It has dimensions $(2\farcs63 \pm 0\farcs20) \times (1\farcs52 \pm 0\farcs06)$ and is therefore also extended. Its nondetection at 3 cm strongly suggests nonthermal emission and may be caused by colliding winds. Strangely, star C does not appear to be a strong radio source, in contrast to its outstanding X-ray flux. This implies that in OB stars, the X-ray and radio emission mechanisms are not always highly correlated (Waldron et al. 1998).

[14] Since no pileup corrections were applied, the L_X values for the X-ray brightest stars (C, 68, A1+A2+A3) will be lower limits. However, even in the worst case, star C is estimated to be a factor of ~2 too low in L_X, which is ~negligible in the context of Fig. 4 and its implications.

7. No statistically significant X-ray variability is seen exceeding 3 σ (where σ is based on Poisson statistics in a given bin) among any of the 10 individual, resolved, bright (down to ~100 counts total) X-ray sources in Figure 1 (*left*) on timescales of 0.5–50 ks. This was determined by comparing the standard deviation of the X-ray counts about the mean, in eight equal bins, with their instrumental errors, dominated by Poisson statistics. Counts were summed in circles of diameter 7″ outside and 3″ inside the central core of Figure 2.

3.3. *Diffuse X-Ray Emission*

Preliminary reduction (adaptive filtering and deconvolution) of the original X-ray image reveals the presence of weak extended X-ray emission in the immediate surroundings of the cluster core. To enhance the visibility and to quantify this diffuse component, we applied two different approaches. Both approaches attempted to subtract all recognizable point sources using image statistics derived in subrasters, with special attention paid to spatial variability of the background level.

In the first method, each source found by the CIAO WAVDETECT routine[15] was fit with an elliptical Gaussian model convolved with the *Chandra* point-spread function (PSF; generated assuming a single-temperature, absorbed thermal spectrum with $N_H = 1.3 \times 10^{22}$ cm^{-2} and $kT = 0.85$ keV).[16] A fit was performed using a 32×32 pixel subraster surrounding each source, including a background model of the general form $B(x, y) = c + ax + by$, with a, b, and c as fitted parameters. In so doing, we assumed that large-scale ($\gg 16''$) background variations prevail, while significant positive fluctuations on small scales would have been automatically detected as sources. We held fixed the fit parameters of serendipitous sources in the subraster except for normalization, thus preventing these sources from biasing the background model. Pixels in the original image were then replaced by the Poissonian deviations computed from the background model whenever the input image pixel intensity exceeded the background model by 50%.

In the second approach, we divided the central 510×510 pixel part of the image into nine equal subsections, in order to address the issue of gradual variations in the background. We used a PSF constructed from a combination of bright, isolated point sources in the original image, with stars MTT 68 and MTT 71 as the main constituents. (Pileup for MTT 68 and MTT 71 will have negligible impact on the results.) The specially designed source-recognition routine as described in § 3.2 was then run on the whole 510×510 region.

By slightly varying the detection threshold around the 3 σ level (~10 counts per source), we obtained σ-dependent lists of sources, subsequently compiling them via cross-referencing into a final list. Then, a properly scaled PSF was subtracted from each point source contained in the final list until, after several iterations, the locally calculated (10×10 pixel subraster) flux density matched the corresponding average value in each of nine subsections on the original X-ray image. This average value was also recalculated for each

[15] Wavelets are well suited here for identifying structures, including stars, but they are not reliable for obtaining stellar X-ray fluxes, as in § 3.2.

[16] Cf. http://xassist.phys.cmu.edu/ximgfit/manual/node16.html.

iteration to accommodate the changes produced by the source subtraction.

Since both approaches yield comparable results, we combined them by simple averaging into an image with pixels of size $12'' \times 12''$, as shown in Figure 5. Clearly, the high density of sources in the central core reduces the reliability of both techniques there (i.e., inside the region limited by a red circle in Fig. 5). Detailed examination of the diffuse emission in the core will be given in a forthcoming paper. Therefore, we take advantage of the ~Gaussian form of the spatial extension of the diffuse X-ray emission outside the dense core to extrapolate into the core. We thus find that the total integrated diffuse X-ray emission, $\sim 10^{34.3}$ ergs s^{-1} (net unabsorbed, integrated within the central $r \lesssim 2'$ region), constitutes ~20% of the integrated point-source stellar X-ray flux. Both this flux ratio and the observed large extension of the diffuse X-ray emission in NGC 3603 contradict the model of Cantó, Raga, & Rodrigues (2000) applied to similar starburst regions, where the extended X-ray emission is predicted to arise from multiple wind-wind interactions.

To address the possibility that the diffuse emission might be generated by faint point sources falling below the 3 σ detectability level, we obtain a $N(S)$ (number versus source-flux) distribution using all the detectable sources, then extrapolate $N(S)$ to lower fluxes. We ignore the fact that the form of the distribution is not spatially invariant; $N(S)$ tends to change toward the center of the image. This limits the accuracy of our extrapolation to within an order of magnitude. Otherwise, subdivision of the initial image into smaller areas would prevent one from obtaining sufficient statistics for constructing a robust N-S diagram for each region. Uncertainty of the point-source removal in the very central, overcrowded part of the image (defined approximately by the central red circle in Fig. 5) forces us to exclude this region in deriving the $N(S)$ relation. We estimate the number of potential point sources in the area occupied by the diffuse X-ray emission as 1.5×10^3, which is close to the number of active pre–main-sequence (PMS) stars expected in the region. However, such young stars may contribute only $\sim 10^{32.5}$ ergs s^{-1} orders of magnitude below the diffuse background flux. If not directly related to PMS stars, the faint undetected point sources would have accounted for ~25% (or even all, allowing for the large uncertainty in the number of extrapolated faint sources) of the diffuse background.

The intensity of the observed diffuse X-ray component does not contradict the nondetection of any extended radio emission coming from the same volume of space. Indeed, assuming optically thin thermal bremsstrahlung emission with $kT \simeq 2$ keV, a radio flux of $\sim 10^{(-4)}$–$10^{(-5)}$ mJy beam^{-1} at $\lambda = 3$ cm is expected, which is far below the ATCA 1 σ detection limit (0.15 mJy beam^{-1}) of our observations.

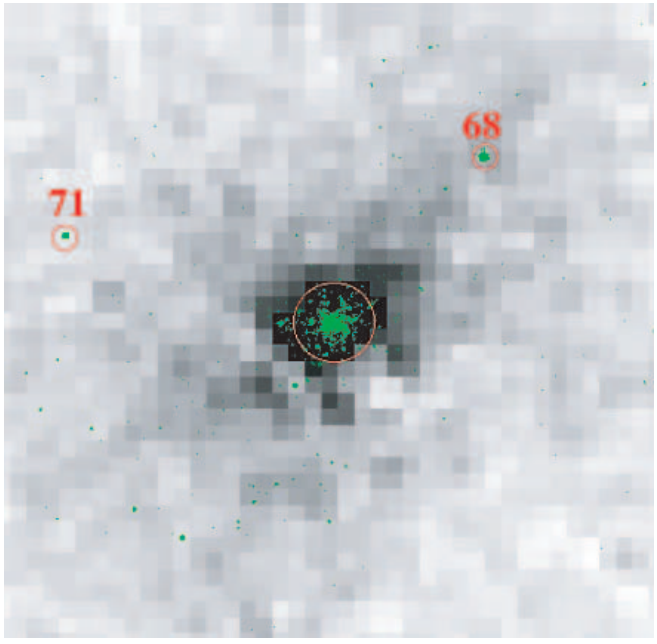

FIG. 5.—*Gray scale*: Rebinned and smoothed central part of the *Chandra*/ACIS-I image. All point sources (in green, from the raw X-ray image) were removed to reveal the extended, diffuse X-ray component. Two point sources are labeled in accordance with Fig. 1.

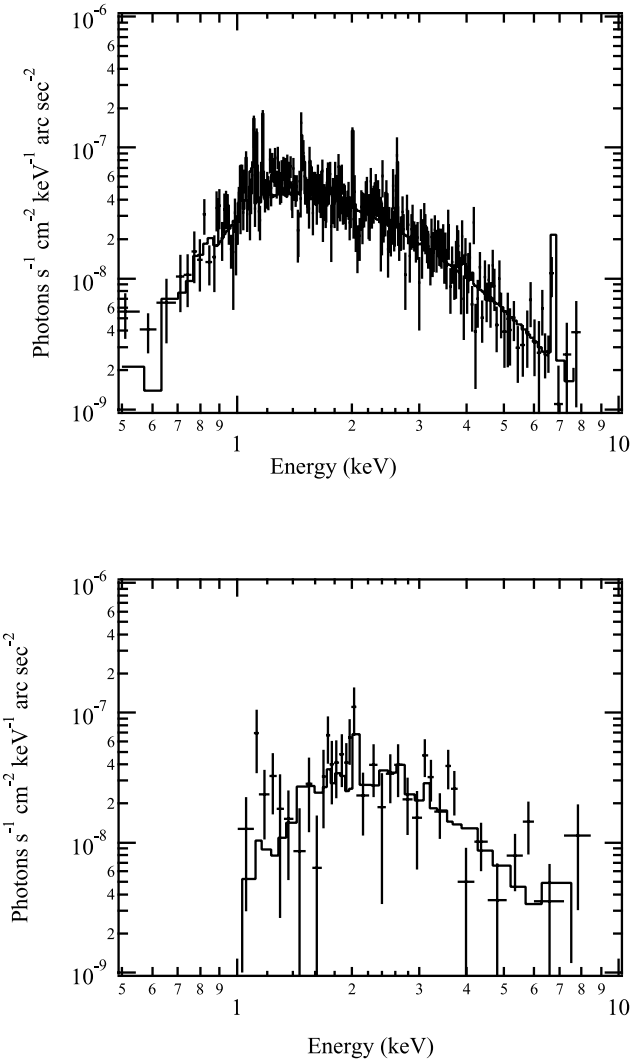

FIG. 6.—Integrated diffuse component of X-ray surface brightness spectra at two locations near NGC 3603. The top plot is the spectrum in a circular annulus centered near star C at the center of the cluster and extending from 7″ to 22″, excluding obvious stellar sources. The bottom plot shows the spectrum in a circular region of radius 12.″3 centered to the southeast of star 68 at $\alpha = 11^h15^m02^s$; $\delta = -61°14'53''$. The solid histograms show the best-fit models as described in the text.

We have extracted (Fig. 6) the integrated diffuse X-ray component spectrum in an annulus around the core region (excluding obvious stellar sources) and a region beyond the core to the southeast of star MTT 68. We fitted each region with a single-temperature absorbed thermal model (Mewe, Gronenschild, & van den Oord 1985; Mewe, Lemen, & van den Oord 1986; Kaastra 1992; and including the updated Fe L emission calculations by Liedahl, Osterheld, & Goldstein 1995). With reduced $\chi^2 = 1.28$, the X-ray temperature of the core is $kT \approx 3.1 \pm 0.3$ keV, compared to $kT \approx 2.1 \pm 0.7$ keV in the outer region. The core also had a lower X-ray absorbing column, $N_{\rm H} \approx 0.7 \times 10^{22}$ cm^{-2} versus $N_{\rm H} \approx 2.4 \times 10^{22}$ cm^{-2} in the outer region of the field; this is compatible with the increase in $E(B-V)$ going out from the core (Melnick et al. 1989).

As an additional independent check on the reality of the weak extended emission component, we performed a census of all the pointlike sources by varying the detection limit (namely, 3, 5, and 10 σ in accordance with Gehrels 1986), and we plot in Figure 7 the integrated, normalized source flux and source number as a function of distance from the tentative center of the cluster (placed at star C for convenience). There is an apparent excess of weak (3–5 σ) sources toward the center of the cluster at $r \lesssim 1'$–$1'.5$, which can be used as an additional argument backing the reality of the X-ray halo.

3.4. *Star Formation and Proplyd-like Objects*

As found in previous lower resolution work (de Pree, Nysewander, & Goss 1999), most of the centimeter radio emission comes from extended regions well outside the central core, i.e., mostly anticorrelated with the X-ray emission. In particular, mostly thermal radio emission is seen from large numbers of clumps of various sizes toward the west-southwest and south-southeast from the central core, at projected distances of ~30″–90″ (1–3 pc; Fig. 1 [*left*]). These are associated with regions of active star formation, with the most intense near-IR/radio flux coming from two giant pillar-head ionization fronts at ~35″ from the cluster core. These pillar heads are also sources of OH and H_2O masers. Inside this radius, there is very little gaseous emission of any kind, except for a diffuse X-ray component from near the core where the hot stellar winds are emerging (Fig. 5). The size of this windblown cavity suggests an age less than 1 Myr (Drissen 1999), in agreement with recent estimates of the nuclear age of the central cluster, e.g., $\leq$1.0 Myr from evolution of the massive stars (Pandey, Ugura, & Sekiguchi 2000) or 0.3–1.0 Myr from PMS evolution (Brandl et al. 1999). Near the southern end of the southern giant pillar is located an embedded, very young star cluster (E. Grebel 2001, private communication). It appears to be a compact IR/radio source that lies between two adjacent *Chandra* point sources. This will be discussed in a future paper.

In addition to these extended regions, the three proplyd-like structures detected at near-IR wavelengths (Brandner et al. 2000) are resolved as very strong, extended centimeter radio sources (see Fig. 1), with both thermal and nonthermal components. The NGC 3603 proplyd-like objects are the most massive, luminous, and distant of their kind discovered so far and the only ones in which magnetic processes are inferred because of their nonthermal components (Mücke et al. 2002a). In the meantime, a fourth proplyd-like object has been identified in NGC 3603 (Mücke et al. 2002b). However, it appears to have more the appearance of a minipillar.

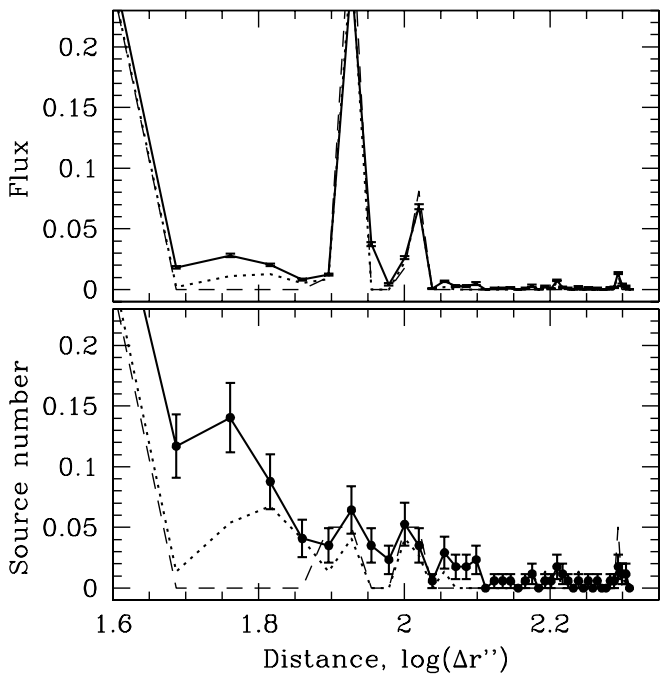

FIG. 7.—Integrated, normalized source flux (*top panel*) and source number (*bottom panel*) as a function of the distance from the approximate center of the cluster (star C). The solid line shows all the sources detected at $\geq$3 σ level, the dotted line corresponds to $\geq$5 σ, and the dashed line shows the $\geq$10 σ sources.

4. INTEGRATED PROPERTIES AND COMPARISON WITH OTHER STARBURSTS

The net instrumental background-corrected count rate from the entire ACIS-I observation is ~1 count s^{-1}. Assuming a 3 keV thermal spectrum with $N_{\rm H} = 7 \times 10^{21}$ cm^{-2} and a distance of 7 kpc, the total luminosity in the 0.5–10 keV band of NGC 3603 in the ACIS-I field of view is $L_{\rm X}$ (0.5–10 keV) $= 3 \times 10^{34}$ ergs s^{-1} (net observed) or 1×10^{35} ergs s^{-1} (net unabsorbed).

With time, the massive stellar population will evolve and eventually explode as supernovae, producing X-ray–bright supernova remnants and compact objects, so that the integrated X-ray luminosity from the region will increase (Van Bever & Vanbeveren 2000). Other older, well-studied starbursts such as 30 Dor in the LMC and M82 show X-ray emission dominated by supernova remnants (SNRs) and collapsed objects. The integrated luminosity of 30 Dor measured by *ROSAT* is $\approx 6 \times 10^{37}$ ergs s^{-1} in the 0.1–2.4 keV band, with only 1%–2% of the emission produced by unevolved massive stars (Norci & Ogelman 1995). The X-ray temperature of 30 Dor from the *ROSAT* observations, however, is only 0.3–0.4 keV, significantly lower than the temperature of NGC 3603 measured by *Chandra*. *ASCA* observations of the canonical starbursts M82 (Tsuru et al. 1997) and NGC 253 (Ptak et al. 1997) showed that these systems contain distinct hard and soft emission components, with the hard component being more centrally concentrated. These results were confirmed by *Chandra* (Griffiths et al. 2000) and *XMM-Newton* (Pietsch et al. 2001) observations, which found that most of the hard component can be attributed to multiple (often variable) point sources and an

extended nuclear component (at temperatures on the order of 5–10 keV), whereas the soft component is due to disk emission and a superwind outflow. As has been known from *ROSAT* PSPC and HRI observations (Strickland, Ponman, & Stevens 1997), the disk/superwind emission in these systems tends to have a temperature of the order of $\sim$1 keV, decreasing to $\sim$0.4 keV in the halo, and X-ray enhancements in the vicinity of known H II regions are often observed (e.g., M51 in Marston et al. 1995). It is therefore possible that some fraction of the ($L_X \sim 10^{40}$ ergs s^{-1}) disk emission in starburst galaxies is due to $\lesssim 10^5$ NGC 3603–type H II regions, while the bulk of the hot interstellar matter (ISM) outside their nuclei has expanded and cooled to lower temperatures than those found in NGC 3603.

5. SUMMARY AND CONCLUSIONS

The most important findings of this work are:

1. While its more luminous member stars reveal a general trend between L_X and L_{bol} as seen in other less exotic clusters, the scatter is enormous and definitely intrinsic to the stars. Some of the X-ray overluminous sources may indicate the presence of colliding winds in binaries.

2. The three W-R stars appear anomalously bright in L_X compared to other W-R stars. Probably, these are not ordinary W-R stars, but rather, extremely luminous main-sequence stars with winds of relatively low X-ray opacity. Another factor that could enhance their L_X flux is colliding-wind emission in the two W-R stars that are suspected to be binary.

3. Large numbers of X-ray sources are found with greater frequency toward the cluster center and no obvious optical counterparts. If these sources are cluster members, then they may be active, low-mass PMS stars, although other types of high L_X/L_{bol} objects cannot be entirely ruled out (for example, some of them might be isolated neutron stars or heavily embedded X-ray binaries).

4. Spatially integrated X-ray spectra reveal that N_H increases along with $E(B-V)$ as one goes from the cluster core to the periphery, as is expected for a windblown cavity of cooler gas and dust evacuated by an ensemble of very hot stars.

5. No significant variability of individual X-ray sources was found on timescales ranging from 0.5 to 50 ks.

6. Central diffuse X-ray emission may arise from multiple merging/colliding hot stellar winds, with negligible contribution from unresolved PMS stars.

7. Most of the centimeter radio emission arises from peripheral regions of current star formation, with little or no correlation with X-rays. However, an extended, possibly nonthermal component (due perhaps to colliding winds) is also present in the central cluster region.

8. NGC 3603 appears to be a somewhat younger and hotter scaled-down version of typical starbursts found in other galaxies.

In a future paper, we will discuss our recent *Chandra* images of the SMC's youngest, dense cluster NGC 346 at 0.1 solar abundance (e.g., Massey, Parker, & Garmany 1989) for comparison with NGC 3603 at solar abundance.

A. F. J. M. is grateful for financial aid from NSERC (Canada) and FCAR (Québec). We gratefully acknowledge financial support provided by NASA and the *Chandra* project (award GO0-1047Z). This research has made use of software obtained from the High Energy Astrophysics Science Archive Research Center (HEASARC), provided by NASA's Goddard Space Flight Center, as well as software distributed by the *Chandra* X-Ray Center. This research has made use of NASA's Astrophysics Data System Abstract Service. We also would like to acknowledge the help and expertise of the scientists at the *Chandra* X-ray Center for their support during this observation. A. M. acknowledges a postdoc bursary from the Québec Government. We thank an anonymous referee for helpful comments.

REFERENCES

Berghöfer, T. W., Schmidt, J. H. M. M., Danner, R., & Cassinelli, J. P. 1997, A&A, 322, 167
Bohlin, R. C., Savage, B. D., & Drake, J. F. 1978, ApJ, 224, 132
Brandl, B., Brandner, W., Eisenhauer, F., Moffat, A. F. J., Palla, F., & Zinnecker, H. 1999, A&A, 352, L69
Brandner, W., Chu, Y.-H., Eisenhauer, F., Grebel, E. K., & Points, S. D. 1997, ApJ, 489, L153
Brandner, W., et al. 2000, AJ, 119, 292
Cantó, J., Raga, A. C., & Rodrígues, L. F. 2000, ApJ, 536, 896
Chlebowski, T., Harnden, F. R., & Sciortino, S. 1989, ApJ, 341, 427
Corcoran, M. F., et al. 1994, ApJ, 436, L95
Crowther, P. A., & Dessart, L. 1998, MNRAS, 296, 622
De Koter, A., Heap, S. R., & Hubeny, I. 1997, ApJ, 477, 792
de Pree, G. G., Nysewander, M. C., & Goss, W. M. 1999, AJ, 117, 2902
Drissen, L. 1999, Proc. IAU Symp. 193, Wolf-Rayet Phenomena in Massive Stars and Starburst Galaxies, ed. K. A. van der Hucht, G. Koenigsberger, & P. R. J. Eenens (San Francisco: ASP), 403
Drissen, L., Moffat, A. F. J., Walborn, N. R., & Shara, M. M. 1995, AJ, 110, 2235
Gehrels, N. 1986, ApJ, 303, 336
Griffiths, R., et al. 2000, Science, 290, 1325
Kaastra, J. S. 1992, An X-Ray Spectral Code for Optically Thin Plasmas (updated version 2.0; Leiden: Internal SRON-Leiden Report)
Kudritzki, R. P., Pauldrach, A., & Puls, J. 1987, A&A, 173, 293
Liedahl, D. A., Osterheld, A. L., & Goldstein, W. H. 1995, ApJ, 438, L115
Marston, A., Elmegreen, D., Elmegreen, B., Forman, W., Jones, C., & Flanagan, K. 1995, ApJ, 438, 663
Massey, P., Parker, J. W., & Garmany, C. D. 1989, AJ, 98, 1305
Melnick, J., Tapia, M., & Terlevich, R. 1989, A&A, 213, 89
Mewe, R., Gronenschild, E. H. B. M., & van den Oord, G. H. J. 1985, A&AS, 62, 197
Mewe, R., Kaastra, J. S., & Liedahl, D. A. 1995, Legacy, 6, 16
Mewe, R., Lemen, J. R., & van den Oord, G. H. J. 1986, A&AS, 65, 511
Moffat, A. F. J. 1983, A&A, 124, 273
Moffat, A. F. J., Drissen, L., & Shara, M. M. 1994, ApJ, 436, 183
Moffat, A. F. J., & Niemela, V. S. 1984, ApJ, 284, 631
Mücke, A., Koribalski, B. S., Moffat, A. F. J., Corcoran, M. F., & Stevens, I. R. 2002a, ApJ, 571, 366
———. 2002b, ESO Workshop on the Origin of Stars and Planets: The VLT View, ed. J. Alves & M. McCaughren (Heidelberg: Springer), in press
Norci, L., & Ogelman, H. 1995, A&A, 302, 879
Pandey, A. K., Ugura, K., & Sekiguchi, K. 2000, PASJ, 52, 847
Pietsch, W., et al. 2001, A&A, 365, L174
Ptak, A., Serlemitsos, P., Yaqoob, T., Mushotzky, R., & Tsuru, T. 1997, AJ, 113, 1286
Schulz, N. S., Canizares, C., Huenemoerder, D., Kastner, J. H., Taylor, S. C., & Bergstrom, E. J. 2001, ApJ, 549, 441
Seward, F. D., & Chlebowski, T. 1982, ApJ, 256, 530
Strickland, D., Ponman, T., & Stevens, I. 1997, A&A, 320, 378
Townsley, L. K., Broos, P. S., Garmire, G. P., & Nousek, J. A. 2000, ApJ, 534, L139
Tsuru, T., Awaki, H., Koyama, K., & Ptak, A. 1997, PASJ, 49, 619
Van Bever, J., & Vanbeveren, D. 2000, A&A, 358, 462
Waldron, W. L., Corcoran, M. F., Drake, S. A., & Smale, A. P. 1998, ApJS, 118, 217
Wessolowski, U. 1996, Proc. Röntgenstrahlung from the Universe, ed. H. U. Zimmermann, J. Trümper, & H. Yorke (MPE Rep. 263; Garching: MPE), 75
Wright, A. E., & Barlow, M. J. 1975, MNRAS, 170, 41